Journal of Materials Chemistry

Cite this: J. Mater. Chem., 2012, 22, 975

www.rsc.org/materials

PAPER

Direct growth of monodisperse SnO_2 nanorods on graphene as high capacity anode materials for lithium ion batteries†

Chaohe Xu, Jing Sun* and Lian Gao*

Received 22nd August 2011, Accepted 18th October 2011
DOI: 10.1039/c1jm14099j

We developed a facile one-step hydrothermal procedure to prepare hybrid materials of SnO_2 nanorods on graphene sheets (GS). Composites with individual SnO_2 nanorods of 10–20 nm in diameter and 100–200 nm in length show a high reversible specific capacity and outstanding cycling stability (710 mAh g^{-1}) as anode materials for lithium ion batteries. Owing to the enhanced lithium storage properties, the SnO_2/GS hybrid could be a promising candidate material for a high-capacity, low cost and environmentally friendly anode for lithium ion batteries (LIBs). This one-step hydrothermal procedure provides a facile technique for the design and morphology control of nanocrystals on GS and will be a versatile route in producing metal oxide/GS composites.

Introduction

Two-dimensional graphene sheets (GS), a monolayer of carbon atoms arranged in a honeycomb network, have received intensive attention due to their unique electrical and mechanical properties, large surface areas, high chemical stability and tunable surface functionalization.[1–3] GS are a potential host material for the homogenous growth of desired active guest materials, such as polymers[4–6] and nanocrystals,[7–9] since the tunable surface functional groups, such as carboxyl and hydroxyl, can act as favorable nucleation sites for the guest materials.[2,10,11] For example, polyaniline[5,12] and polypyrrole[13] have been fabricated by *in situ* chemical polymerization with sheet- and wire-like nanoarchitectures, respectively. CdS and CdSe quantum dots have also been successfully decorated onto GS and showed enhanced physical properties.[14–17] In addition, the composites of GS and metal oxides have been synthesized by many chemical procedures, such as *in situ* chemical synthesis and the self-assembly method.[8,18–20] Although the decoration of nanostructures on GS has been widely investigated, it remains highly desirable and a great challenge to synthesize nanocrystals with specific morphologies on GS due to the micro-heterogeneous system of the graphene oxide (GO) or GS colloidal solution. Unlike the homogeneous solution, physical morphology and crystalline of nanocrystals could be easily controlled in the nucleation and growth processes.[21–26] It is more difficult to synthesize nanocrystals with controllable morphologies in the heterogeneous nucleation process. Although metal oxide nanowires and nanoarrays attached on GS have been reported[27–32] and applied as anode materials for LIBs,[7,9] it is still very challenging to explore methods to deposit nanocrystals with a specific morphology onto GS directly.

Nanostructured tin oxide materials have attracted wide research attention as a negative electrode material for LIBs due to their high theoretical capacity, low cost and widespread availability. In a SnO_2-based LIB electrode, there are two electrochemical processes. The first reaction is responsible for the irreversible capacity loss of the first cycle due to the formation of inactive Li_2O, which can explain the large irreversible capacity loss in the first cycle;[33,34] the second is a reversible process with lithium insertion and extraction between Li_xSn ($0 \leq x \leq 4.4$) and Sn.[35–39] The theoretical capacity of SnO_2 based electrode materials was calculated to be 782 mAh g^{-1}, which is more than twice of graphite.[37,39] However, the large volume variation during the discharge/charge process results in pulverization of the electrode materials which may destroy their close electrical contact with the current collectors and lead to rapid capacity loss and poor cycling stability. To achieve high specific capacity and cyclic stability, composites based on SnO_2 have been widely investigated in recent years because of their potential to integrate the unique properties of both components. Among these, carbonaceous materials have attracted considerable interest owing to their high electrical conductivity, large surface area and fair mechanical properties.[40–43] For example, SnO_2/MWCNT composites with SnO_2 nanoparticles coated onto the surface and filled into the inner cavities of MWCNTs exhibit enhanced lithium storage properties.[39] And also, dense core–shell structured SnO_2/C composites are prepared as anode materials and deliver a high capacity of ~630 mAh g^{-1} at 100 mA g^{-1} even after 50 cycles.[44] Nearly mono-dispersed carbon coated SnO_2 nanocolloids have also been synthesized and their capacity remained

The State Key Lab of High Performance Ceramics and Superfine Microstructure, Shanghai Institute of Ceramics, Chinese Academy of Sciences, 1295 Dingxi Road, Shanghai, 200050, P.R. China. E-mail: jingsun@mail.sic.ac.cn; liagao@mail.sic.ac.cn; Fax: +86-21-52413122; Tel: +86-21-52414301

† Electronic Supplementary Information (ESI) available: TEM, SEM and additional experimental data. See DOI: 10.1039/c1jm14099j/

as high as 440 mAh g^{-1} after 100 cycles.[43] Graphene, a new type of two-dimensional monolayer carbon material, has been also introduced to improve the lithium storage properties of SnO_2. For example, nanoporous SnO_2/GS composites have been achieved by an interface reassembled method and remained 570 mAh g^{-1} after 15 cycles at 60 mA g^{-1}. Liu and coworkers have developed a ternary self-assembly approach using GS as fundamental building blocks to construct ordered SnO_2/GS composites, which showed a steady specific capacity of 625 mAh g^{-1} at 10 mA g^{-1} after 10 cycles.[45] The SnO_2/GS composites have been synthesized by *in situ* chemical methods. However, strong reducing agents such as hydrazine and sodium borohydride were widely used in the chemical reduction of GO to GS. Considering the toxicity and risk of the strong reducing reagents, it is highly desirable to develop a green chemical route for the synthesis of nanocrystals on GS with high conductivity and controllable morphology.

Herein, we have developed a facile one-step hydrothermal procedure to prepare hybrid materials of SnO_2 nanorods on GS, in which the SnO_2 nanorods are uniformly decorated on or encapsulated in GS. The hybrid materials showed a high specific capacity and cycling stability. This one-step hydrothermal procedure provides a facile technique for the design and morphology control of nanocrystals on GS and will be a versatile route to prepare well controlled metal oxide/GS composites.

Experimental details

Materials

Graphite was purchased from Alfa Aesar (-325 mesh). All chemicals were of analytical grade and used without further purification.

Synthesis of graphene oxide (GO)

GO was prepared from graphite flakes by a modified Hummers method.[46,47] 1.0 g of graphite flakes, 1.0 g of $NaNO_3$ and 46 mL of concentrated H_2SO_4 were mixed together in an ice bath for 4 h. Then 6.0 g of $KMnO_4$ was added slowly into the solution. Afterwards, the ice bath was removed and the suspension was stirred for another 4 days. Then the suspension was further treated with 200 mL of warm water (~60 °C) and 10 mL of H_2O_2 (30%). The mixture was centrifuged at 4000 rpm and washed with diluted HCl and water to neutral. Finally, a homogeneous GO aqueous dispersion (1 mg mL^{-1}) was obtained for further use.

Synthesis of SnO_2/GS composites

The composites of SnO_2 nanorods on GS were synthesized simply by a direct hydrothermal method. Briefly, 50 mg of stannic chloride hydrate ($SnCl_4 \cdot 5H_2O$) dissolved into 40 mL of 1 mg mL^{-1} GO aqueous dispersion and was vigorously stirred for 10 min. Afterward, 2 mL of concentrated HCl was added into the above suspension. Then, the mixed suspension was transferred to 50 mL Teflon lined stainless steel autoclaves for a hydrothermal reaction at 120 °C for 24 h. The free SnO_2 nanorods were prepared by the same process.

Characterization methods

Transmission electron microscopy (TEM) was performed on the JEM-2100F Electron Microscope with an accelerating voltage of 200 kV. Field-emission scanning electron microscopy (FE-SEM) was performed on a JSM-6700F at an acceleration voltage of 10.0 kV. FT-IR and Raman spectra were recorded on a Nicolet iZ10 and DXR Raman Microscope with a 532 nm excitation length, Thermal Scientific Co., USA, respectively.

The electrochemical properties of the SnO_2/GS composites as the negative electrode used in Li-ion batteries were characterized at room temperature. The working electrode was prepared from the mixture of the active materials, carbon black (super P) and polyvinylidene fluoride (PVDF) binder in weight ratio of 80 : 10 : 10. Li foil was used as the counter electrode. The electrolyte was 1 M $LiPF_6$ in a 50 : 50 w/w mixture of ethylene carbonate (EC) and dimethyl carbonate (DMC). Cell assembly was carried out in a glovebox with the concentrations of moisture and oxygen below 1 ppm. The electrode activities were measured using a CT2001 battery tester. The cell was charged and discharged at different current densities and the fixed voltage limits between 3.0 V and 10 mV. All the electrochemical experiments were carried out using Parstat 2273 electrochemical station (Princeton applied research CO., Ltd, USA). The cyclic voltammograms of SnO_2/GS composites were carried out using a Parstat 2273 electrochemical station (Princeton applied research CO., Ltd, USA) at a scan rate of 0.5 mV s^{-1} and cycles with voltage window between 3.0 and 0.0 V (*vs.* Li^+/Li).

Results and discussion

Hydrothermal dehydration has been adopted for the green reduction of GO and preparation of nanocrystals on GS.[48,49] Based on this method, we herein develop a novel strategy to synthesize nanosized SnO_2/GS composites with controllable morphologies. A hybrid material with SnO_2 nanorods that grew on the surface of GS was achieved successfully by a facile one-step hydrothermal procedure (Scheme 1). Firstly, ions of Sn^{4+} were anchored covalently to the surface of GO with functional groups such as carboxyl, hydroxyl and epoxy groups through electrostatic interactions. Then, hydrothermal treatment at 120 °C for 24 h was applied to prepare the SnO_2/GS composites.

After reaction, GO was converted to GS in the hydrothermal dehydration process as evidenced by XRD curves (Fig. S1 and the bold curve in Fig. 1a). Due to the presence of oxygenated functional groups on carbon nanosheets, the *d*-spacing of GO calculated from the (001) peak is approximately 0.74 nm (2θ = 11.4°), which is larger than that of graphite (0.34 nm). After 24 h of hydrothermal treatment, a broad peak at ~25° appeared, indicating the further reduction of GO as shown in Fig. 1a. The XRD patterns of the composites clearly show the good

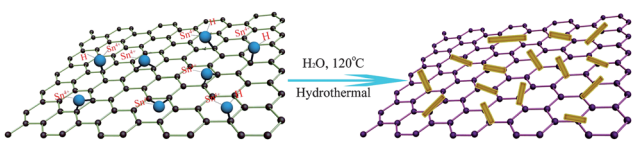

Scheme 1 Schematic diagram of the one-step hydrothermal synthesis of SnO_2/GS.

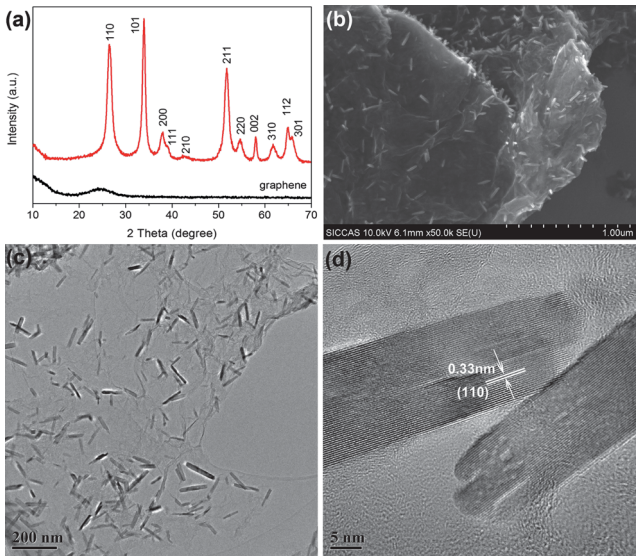

Fig. 1 (a) Characterization of SnO_2/GS composites. (a) XRD curves of the as synthesized GS and SnO_2/GS composite. (b) SEM image of SnO_2/GS composites. (c) TEM image of SnO_2/GS composites. (d) High-resolution TEM image of SnO_2 nanorods on GS.

crystallization of tetragonal SnO_2 (t-SnO_2, JCPDS card no. 41–1445; red curve in Fig. 1a). The diffraction peak at 25° of GS overlapped with the (110) peak of SnO_2. As shown in SEM and TEM images (Fig. 1b–d and Fig. S3), the SnO_2 nanorods were uniformly decorated on the surface of GS with the sizes of 10–20 nm in diameter and 100–200 nm in length. The high-resolution TEM image (Fig. 1d) shows that the crystal lattice fringe is 0.33 nm, corresponding to the (110) face of t-SnO_2. Fig. 2 exhibits the thermal stability of SnO_2/GS using thermogravimetric (TG) analysis. The weight loss of 7.2 wt% around 100 °C was ascribed to the absorbed water of the SnO_2/GS composites. And the weight loss of 51.94 wt% between 200–650 °C was ascribed to decomposition of labile oxygen groups (carboxyl, anhydride or lactone groups) and the removal of more stable oxygen groups (phenol, carbonyl or quinone) on GS, respectively. The high exothermal peak, in agreement with previous reports,[50,51] is attributed to C–C bonds and the most stable functionalities that cannot be removed even after a prolonged hydrothermal reduction process. The mass loading of SnO_2 calculated was 44 wt% in the SnO_2/GS composites.

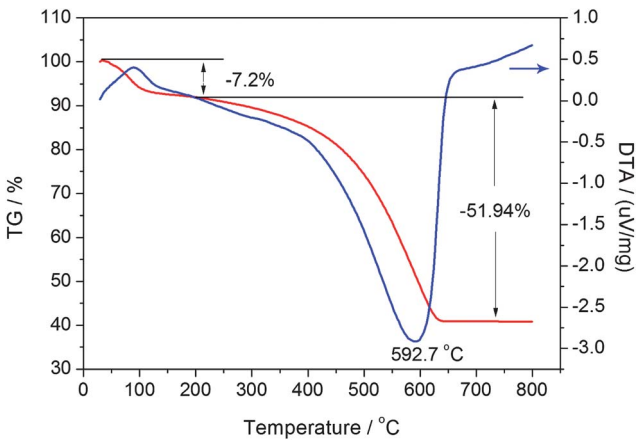

Fig. 2 TG-DTA curves of SnO_2/GS composites. There is ~7.2% weight loss attributed to dehydration of SnO_2/GS composites.

Fig. 3 shows the Fourier transformation infrared (FT-IR) and Raman spectra of SnO_2/GS composites. A red shifts was observed in the FT-IR spectra of SnO_2/GS composites with respect to that of pure SnO_2 nanorods (Fig. 3a), which was attributed to the electron-donating effect of GS (n-type doping effect). As shown in Fig. 3b, the G bands in the Raman spectrum of the SnO_2/GS composites exhibit blue shifts compared with GO and GS, which revealed the p-type doping effect on GS (electron-withdrawing effect). The G band is usually assigned to the E_{2g} phonon of C sp^2 atoms, while the D band is the breathing mode of κ-point phonons of A_{1g} symmetry. A prominent D band is an indication of a disordered carbon structure in GO, originated from defects associated with vacancies, grain boundaries and amorphous carbon species. The intensity ratio (I_D/I_G) of D band to G band is related to the extent of π-conjugation and concentration of defects, which are 1.23, 1.32 and 1.39, respectively, for GO, GS and SnO_2/GS. The red shift of the FT-IR of SnO_2, blue shifts of the G bands of GS and the different I_D/I_G revealed the electronic interactions between SnO_2 nanorods and GS, which is beneficial for electron transportation between SnO_2 and GS and the formation of the three-dimensional electron networks is desirable for lithium storage.

Fig. 4a shows the cyclic voltammetry (CV) curves of the SnO_2/GS electrode at the constant scan rate of 0.5 mV s^{-1} in the 1st, 2nd, 3rd, 4th and 5th cycle with voltage window between 3.0 and 0.0 V (*vs.* Li^+/Li). In the first cycle, the cathodic peak at ~0.7 V can be attributed to the formation of the solid electrolyte interphase (SEI) layer ($4Li^+ + SnO_2 + 4e^- = Sn + 2Li_2O$).[37] The lithium reaction with SnO_2 and GS occurred at ~0.12 and 0.01 V ($xLi^+ + Sn + xe^- = Li_xSn$; $xLi^+ + C(GS) + xe^- = Li_xC$).[43] Three oxidation peaks appear around 0.15, 0.55 and 1.25 V, respectively. The anodic peak at 0.15 V corresponds to lithium extraction from GS; the 0.55 V oxidation peak can be assigned to the de-alloying of Li_xSn, while the weak oxidation peak at 1.25 V could be partially reversible reaction of formation of SEI layer. The 2nd, 3rd, 4th and 5th cycles stack together which clearly elucidate the reversible electrochemical reactions between lithium ions and the SnO_2/GS hybrid materials.

Fig. 4b–c show the discharge/charge curves of the SnO_2/GS hybrid materials at a current density of 100 and 200 mA g^{-1}, respectively. The capacity corresponding to voltage range of ~1.0 to 0.5 V of the first Li^+ charge curve can be attributed to the

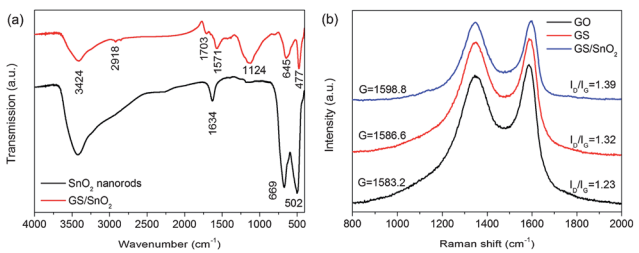

Fig. 3 (a) FT-IR spectra of SnO_2/GS composites and pure SnO_2 nanorods; (b) Raman spectra of GO, GS and SnO_2/GS composites.

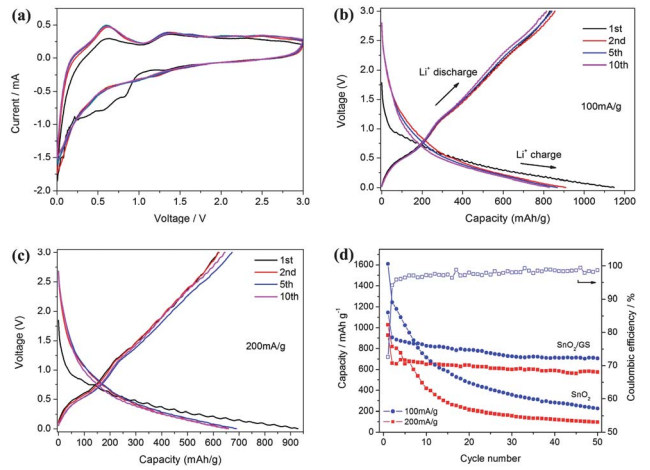

Fig. 4 Electrochemical characterizations of GS/SnO_2 composites. (a) Cyclic voltammograms of SnO_2/GS composites, the scan rate is 0.5 mV s^{-1}. (b–c) The discharge/charge profiles of GS/SnO_2 composites at current densities of 100 and 200 mA g^{-1}, respectively. (d) The discharge/charge capacity profiles of GS/SnO_2 composites and pure SnO_2 nanorods in 5 mV–3 V (*vs.* Li^+/Li) voltage window at current densities of 100 and 200 mA g^{-1}, respectively.

irreversible reaction of the formation of SEI layer.[19] The Li^+ discharge curves show a sloping plateau at ~1.25 V due to the partially reversible reaction of formation of SEI layer. It is very consistent with the CV curves in Fig. 4a. The initial discharge capacities are 1147 and 928 mAh g^{-1} at current densities of 100 and 200 mA g^{-1}, respectively. After several discharge/charge cycles, the coulombic efficiency of the hybrid electrodes increases to greater than 98% (Fig. 4b and c), and indicating good reversibility of the above electrochemical reactions.

Fig. 4d show cyclic performance and coulombic efficiency of the hybrid electrode. The second discharge capacities are 907 and 659 mAh g^{-1} at current densities of 100 and 200 mA g^{-1}, respectively, which retained about 79 and 71% of the initial capacities. After 50 cycles, the capacities are 710 and 574.6 mAh g^{-1} with a capacity loss of ~0.3% per cycle with the current density of 100 and 200 mA g^{-1}, which are superior to that of SnO_2 nanoparticles coated on carbon nanotubes or encapsulated in carbon spheres.[37,39,40,43] Comparisons of the cyclic performance of the composite structures with that of bare SnO_2 nanorods are shown in Fig. 4d and Fig. S4. After 50 cycles, the specific capacities are 237 and 105 mAh g^{-1}, which are much lower than the initial specific capacities (1610 and 1027 mAh g^{-1} at current densities of 100 and 200 mA g^{-1}, respectively). The capacity, rate capability and cycling stability of GS/SnO_2 hybrid materials are superior to the bare SnO_2 nanorods, which can be attributed to the interaction between the SnO_2 nanorods and the GS. The strong interaction between them makes SnO_2 more stable and electrochemically active during the discharge/charge process.[51] The lithium storage properties of the hybrid electrodes are superior to the SnO_2/GS nanoporous composites prepared by reassembled process and ternary self-assembly of ordered SnO_2/GS composites which show discharge capacities only 570 and 625 mAh g^{-1} at current densities of 50 and 10 mA g^{-1}, respectively.[7a,20] These were attributed to the intimate interactions between GS substrates and the SnO_2 nanorods directly grown on them, which could effectively and rapidly transport electrons between SnO_2 and GS to the current collector through the highly conducting three-dimensional GS network.[45,52]

In order to understand the excellent electrochemical performance of the SnO_2/GS composites, their microstructure and morphology after 50 discharge/charge cycles was examined by TEM. As shown in Fig. S5, the SnO_2 nanoparticles were still decorated on GS, which indicated the role of GS to prevent the agglomeration of SnO_2 nanoparticles during cycling. As mentioned above, ions of Sn^{4+} were firstly anchored covalently to the functional groups on GS such as hydroxy, carboxyl and carbonyl *via* electrostatic attraction force. Then, after hydrothermal treatment, the SnO_2 nanorods attached firmly on the GS sheets by covalent bonds (such as Sn–O bonds). This connection has been verified by the FT-IR and Raman shifts. However, SnO_2 nanorods were partially pulverized due to the volume change in the discharge/charge process, which is responsible for the capacity loss with cycling.

Conclusions

In summary, we have developed a facile one-step hydrothermal procedure to prepare hybrid materials of SnO_2 nanorods on GS, in which the SnO_2 are nanorods uniformly decorated on or encapsulated in GS. The hybrid materials showed a high specific capacity and cycling stability, owing to the synergistic effect between the GS and the SnO_2 nanorods. Accordingly, the SnO_2/GS hybrids are potential electrode materials for LIBs. This one-step hydrothermal procedure provides a facile technique for the design and morphology control of nanocrystals on GS and will be a versatile route to prepare well controlled metal oxide/GS composites.

Acknowledgements

This work is supported by the National Natural Science Foundation of China (Grant No. 50972153, 509721157 and 51072215) and Shanghai Municipal Committee of science and technology (Grant No. 10DZ0505000).

Notes and references

1 D. A. Dikin, S. Stankovich, E. J. Zimney, R. D. Piner, G. H. B. Dommett, G. Evmenenko, S. T. Nguyen and R. S. Ruoff, *Nature*, 2007, **448**, 457–460.
2 S. Stankovich, D. A. Dikin, G. H. B. Dommett, K. M. Kohlhaas, E. J. Zimney, E. A. Stach, R. D. Piner, S. T. Nguyen and R. S. Ruoff, *Nature*, 2006, **442**, 282–286.
3 T. Ramanathan, A. A. Abdala, S. Stankovich, D. A. Dikin, M. Herrera-Alonso, R. D. Piner, D. H. Adamson, H. C. Schniepp, X. Chen, R. S. Ruoff, S. T. Nguyen, I. A. Aksay, R. K. Prud'homme and L. C. Brinson, *Nat. Nanotechnol.*, 2008, **3**, 327–331.
4 N. I. Kovtyukhova, P. J. Ollivier, B. R. Martin, T. E. Mallouk, S. A. Chizhik, E. V. Buzaneva and A. D. Gorchinskiy, *Chem. Mater.*, 1999, **11**, 771–778.
5 A. V. Murugan, T. Muraliganth and A. Manthiram, *Chem. Mater.*, 2009, **21**, 5004–5006.
6 L. J. Cote, R. Cruz-Silva and J. X. Huang, *J. Am. Chem. Soc.*, 2009, **131**, 11027–11032.
7 C. Xu, X. Wang, J. W. Zhu, X. J. Yang and L. Lu, *J. Mater. Chem.*, 2008, **18**, 5625–5629.

8 D. H. Wang, D. W. Choi, J. Li, Z. G. Yang, Z. M. Nie, R. Kou, D. H. Hu, C. M. Wang, L. V. Saraf, J. G. Zhang, I. A. Aksay and J. Liu, *ACS Nano*, 2009, **3**, 907–914.
9 Y. C. Qiu, K. Y. Yan, S. H. Yang, L. M. Jin, H. Deng and W. S. Li, *ACS Nano*, 2010, **4**, 6515–6526.
10 S. B. Yang, X. L. Feng, S. Ivanovici and K. Mullen, *Angew. Chem., Int. Ed.*, 2010, **49**, 8408–8411.
11 C. Xu and X. Wang, *Small*, 2009, **5**, 2212–2217.
12 D. W. Wang, F. Li, J. P. Zhao, W. C. Ren, Z. G. Chen, J. Tan, Z. S. Wu, I. Gentle, G. Q. Lu and H. M. Cheng, *ACS Nano*, 2009, **3**, 1745–1752.
13 S. Biswas and L. T. Drzal, *Chem. Mater.*, 2010, **22**, 5667–5671.
14 A. N. Cao, Z. Liu, S. S. Chu, M. H. Wu, Z. M. Ye, Z. W. Cai, Y. L. Chang, S. F. Wang, Q. H. Gong and Y. F. Liu, *Adv. Mater.*, 2010, **22**, 103.
15 X. M. Geng, L. Niu, Z. Y. Xing, R. S. Song, G. T. Liu, M. T. Sun, G. S. Cheng, H. J. Zhong, Z. H. Liu, Z. J. Zhang, L. F. Sun, H. X. Xu, L. Lu and L. W. Liu, *Adv. Mater.*, 2010, **22**, 638–642.
16 C. X. Guo, H. B. Yang, Z. M. Sheng, Z. S. Lu, Q. L. Song and C. M. Li, *Angew. Chem., Int. Ed.*, 2010, **49**, 3014–3017.
17 S. Neubeck, L. A. Ponomarenko, F. Freitag, A. J. M. Giesbers, U. Zeitler, S. V. Morozov, P. Blake, A. K. Geim and K. S. Novoselov, *Small*, 2010, **6**, 1469–1473.
18 S. Q. Chen and Y. Wang, *J. Mater. Chem.*, 2010, **20**, 9735–9739.
19 J. Yao, X. P. Shen, B. Wang, H. K. Liu and G. X. Wang, *Electrochem. Commun.*, 2009, **11**, 1849–1852.
20 S. M. Paek, E. Yoo and I. Honma, *Nano Lett.*, 2009, **9**, 72–75.
21 X. D. Liang, L. Gao, S. W. Yang and J. Sun, *Adv. Mater.*, 2009, **21**, 2068–2071.
22 H. L. Xu and W. Z. Wang, *Angew. Chem., Int. Ed.*, 2007, **46**, 1489–1492.
23 X. G. Han, M. S. Jin, S. F. Xie, Q. Kuang, Z. Y. Jiang, Y. Q. Jiang, Z. X. Xie and L. S. Zheng, *Angew. Chem., Int. Ed.*, 2009, **48**, 9180–9183.
24 X. Liu, Y. D. Deng, B. Shen, L. Liu and W. B. Hu, *Trans. Nonferrous Met. Soc. China*, 2006, **16**, 1184–1188.
25 Y. D. Yin, R. M. Rioux, C. K. Erdonmez, S. Hughes, G. A. Somorjai and A. P. Alivisatos, *Science*, 2004, **304**, 711–714.
26 H. J. Fan, U. Gosele and M. Zacharias, *Small*, 2007, **3**, 1660–1671.
27 S. Chen, J. W. Zhu, X. D. Wu, Q. F. Han and X. Wang, *ACS Nano*, 2010, **4**, 2822–2830.
28 O. Akhavan, *ACS Nano*, 2010, **4**, 4174–4180.
29 O. Akhavan, M. Abdolahad, A. Esfandiar and M. Mohatashamifar, *J. Phys. Chem. C*, 2010, **114**, 12955–12959.
30 D. Choi, M. Y. Choi, W. M. Choi, H. J. Shin, H. K. Park, J. S. Seo, J. Park, S. M. Yoon, S. J. Chae, Y. H. Lee, S. W. Kim, J. Y. Choi, S. Y. Lee and J. M. Kim, *Adv. Mater.*, 2010, **22**, 2187–2192.
31 J. M. Lee, J. W. Choung, J. Yi, D. H. Lee, M. Samal, D. K. Yi, C. H. Lee, G. C. Yi, U. Paik, J. A. Rogers and W. I. Park, *Nano Lett.*, 2010, **10**, 2783–2788.
32 Z. Y. Yin, S. X. Wu, X. Z. Zhou, X. Huang, Q. C. Zhang, F. Boey and H. Zhang, *Small*, 2010, **6**, 307–312.
33 T. Brousse, R. Retoux, U. Herterich and D. M. Schleich, *J. Electrochem. Soc.*, 1998, **145**, 1–4.
34 I. A. Courtney and J. R. Dahn, *J. Electrochem. Soc.*, 1997, **144**, 2045–2052.
35 C. Wang, Y. Zhou, M. Y. Ge, X. B. Xu, Z. L. Zhang and J. Z. Jiang, *J. Am. Chem. Soc.*, 2010, **132**, 46–47.
36 H. X. Zhang, C. Feng, Y. C. Zhai, K. L. Jiang, Q. Q. Li and S. S. Fan, *Adv. Mater.*, 2009, **21**, 2299–2304.
37 X. W. Lou, C. M. Li and L. A. Archer, *Adv. Mater.*, 2009, **21**, 2536–2539.
38 X. W. Lou, D. Deng, J. Y. Lee and L. A. Archer, *Chem. Mater.*, 2008, **20**, 6562–6566.
39 C. H. Xu, J. Sun and L. Gao, *J. Phys. Chem. C*, 2009, **113**, 20509–20513.
40 Z. H. Wen, Q. Wang, Q. Zhang and J. H. Li, *Adv. Funct. Mater.*, 2007, **17**, 2772–2778.
41 G. Chen, Z. Y. Wang and D. G. Xia, *Chem. Mater.*, 2008, **20**, 6951–6956.
42 J. S. Chen, Y. L. Cheah, Y. T. Chen, N. Jayaprakash, S. Madhavi, Y. H. Yang and X. W. Lou, *J. Phys. Chem. C*, 2009, **113**, 20504–20508.
43 X. W. Lou, J. S. Chen, P. Chen and L. A. Archer, *Chem. Mater.*, 2009, **21**, 2868–2874.
44 X. Liu, Y. S. Hu, J. O. Muller, R. Schlogl, J. Maier and D. S. Su, *ChemSusChem*, 2010, **3**, 261–265.
45 D. H. Wang, R. Kou, D. Choi, Z. G. Yang, Z. M. Nie, J. Li, L. V. Saraf, D. H. Hu, J. G. Zhang, G. L. Graff, J. Liu, M. A. Pope and I. A. Aksay, *ACS Nano*, 2010, **4**, 1587–1595.
46 Y. Chen, X. Zhang, P. Yu and Y. W. Ma, *Chem. Commun.*, 2009, 4527–4529.
47 C. H. Xu, J. Sun and L. Gao, *J. Mater. Chem.*, 2011, **21**, 11253–11258.
48 Y. Zhou, Q. L. Bao, L. A. L. Tang, Y. L. Zhong and K. P. Loh, *Chem. Mater.*, 2009, **21**, 2950–2956.
49 H. L. Wang, J. T. Robinson, G. Diankov and H. J. Dai, *J. Am. Chem. Soc.*, 2010, **132**, 3270–3271.
50 M. J. Fernandez-Merino, L. Guardia, J. I. Paredes, S. Villar-Rodil, P. Solis-Fernandez, A. Martinez-Alonso and J. M. D. Tascon, *J. Phys. Chem. C*, 2010, **114**, 6426–6432.
51 J. Z. Wang, C. Zhong, D. Wexler, N. H. Idris, Z. X. Wang, L. Q. Chen and H. K. Liu, *Chem.–Eur. J.*, 2011, **17**, 661–667.
52 H. L. Wang, L. F. Cui, Y. A. Yang, H. S. Casalongue, J. T. Robinson, Y. Y. Liang, Y. Cui and H. J. Dai, *J. Am. Chem. Soc.*, 2010, **132**, 13978–13980.